Steady-State Multiplicity in Cocurrently Cooled Autothermal Reactors

Marisa Pedernera, Daniel O. Borio, and José A. Porras
Planta Piloto de Ingeniería Química (UNS-CONICET), 8000 Bahía Blanca, Argentina

The steady-state simulation of a cocurrently cooled autothermal fixed-bed reactor was carried out using a 2-D heterogeneous mathematical model. The ammonia synthesis was chosen as a case study. Unlike the not-autothermal cocurrent reactor, which is unconditionally stable, the autothermal cocurrent reactor shows multiple steady states within a broad range of operating conditions. This finding, not reported in the literature, is explained through the mass transport from the bottom to the top of the reactor, associated with a feedback of energy. The feedback of heat, which is inherent to autothermal reactors, leads to an ignition-extinction phenomenon similar to that found in the countercurrent configuration. The influence of different parameters on the stability of the autothermal cocurrent reactor was analyzed. The regions where steady-state multiplicity occurs were compared with those presented by the autothermal countercurrent reactor. The influence of an additional heat exchanger on the reactor stability was considered.

Introduction

Starting from the pioneer study of van Heerden (1953), the steady-state multiplicity of countercurrently cooled tubular reactors has been extensively studied (Baddour et al., 1965; Inoue and Komiya, 1968; Luss and Medellin, 1972). It is well known that the autothermal countercurrent reactor can exhibit three steady states for the same operating conditions. In fact, three different temperatures can be obtained at the inlet of the catalyst bed for a given inlet temperature of the coolant (van Heerden, 1953; Baddour et al., 1965). It can be shown that the upper and lower steady states are stable, while the intermediate steady state is unstable. A hysteresis loop appears, associated with a characteristic ignition-extinction behavior. In the particular case of ammonia synthesis, the optimal operating condition corresponds to an upper steady state, located near the extinction point or "blowout" temperature (Baddour et al., 1965; Elnashaie et al., 1988). Several analyses of stability in autothermal countercurrent reactors have been carried out (Ampaya and Rinker, 1977; Chylla et al., 1987; among others). The existence of an arbitrarily large number of steady states has recently been predicted for the autothermal countercurrent reactor (Lovo and Balakotaiah, 1992, 1994).

Correspondence concerning this article should be addressed to D. O. Borio.

The autothermal cocurrent reactor has been markedly less studied than the countercurrent configuration. However, Fodor (1971) suggested that this coolant-flow scheme can achieve a better tracking of the optimal temperature profile for the case of ammonia synthesis. Recently, Pedernera et al. (1996) have demonstrated that the cocurrent design leads to significant improvements in the conversion per pass with respect to the existing industrial designs, provided that an auxiliary heat exchanger is included at the top of the reactor. The stability of the autothermal cocurrent reactor has been analyzed by Degnan and Wei (1979, 1980). These researchers concluded that the autothermal reactor under this particular coolant-flow scheme does not present steady-state multiplicity and therefore would be unconditionally stable. Their finding would not agree with the assertion: "all effects which transport heat from the back to the front of the reactor lead to destabilization" (Eigenberger, 1981). Indeed, feedback effects are clearly found in the countercurrent reactor, but they are also present in the autothermal cocurrent reactor, because the feed stream (after performing as a coolant) is collected and transported to the top of the reactor to enter the catalyst bed (see Figure 1a).

Provided these contradictory opinions about reactor stability, the steady-state simulation of an autothermal reactor used

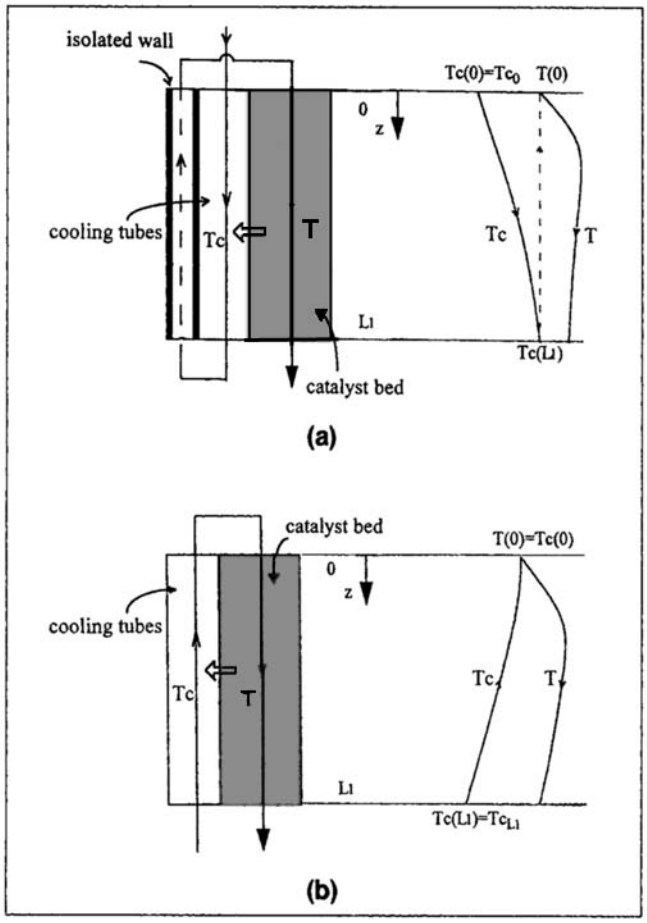

Figure 1. Autothermal reactor: (a) cocurrent; (b) countercurrent.

for ammonia synthesis has been carried out in the present work, with the following objectives:

1. To demonstrate the existence of multiple steady states in the autothermal cocurrent reactor;
2. To compare the zones of multiplicity (or steady-state regions) with respect to those found in the autothermal countercurrent reactor;
3. To investigate the influence of a heat-exchanger (usually located at the bottom of the reactor) on the steady-state regions.

Mathematical Model

A two-dimensional heterogeneous model has been chosen to simulate the steady-state behavior of an autothermal multitubular-shell-side (MSS) fixed-bed reactor. The ammonia synthesis was selected as a case study. The *Equivalent Annular Model* proposed by Li et al. (1991) was adopted to represent the shell-side catalyst bed. According to this model, the cross-sectional area of the catalyst bed is considered to be subdivided into identical annular areas centered around each cooling tube. Two different coolant-flow schemes will be considered: cocurrent flow (Figure 1a) and countercurrent flow (Figure 1b).

On the basis of a previous contribution (Pedernera et al., 1996), the following supplementary assumptions have been made:

i. External transport resistances for mass and heat are neglected;
ii. The catalyst particle is isothermal; the intraparticle mass-transfer restrictions are accounted for by means of an effectiveness factor;
iii. Axial dispersion of heat and mass is neglected;
iv. Constant reactor pressure.

Based on these assumptions, the mass- and heat-balance equations can be written as follows.

Catalyst bed (shell side)

Gas phase:

$$\frac{\partial y_{N_2}}{\partial z} = \frac{M}{G}\left[\frac{1}{r}\frac{\partial}{\partial r}\left(rD_{er}C\frac{\partial y_{N_2}}{\partial r}\right) - \frac{\alpha R_{NH_3}}{2}\eta\right] \tag{1}$$

$$\frac{\partial T}{\partial z} = \frac{M}{G\sum_i y_i c_{pi}}\left[\frac{1}{r}\frac{\partial}{\partial r}\left(rk_{er}\frac{\partial T}{\partial r}\right) + (-\Delta H_r)\alpha R_{NH_3}\eta\right], \tag{2}$$

where

$$\eta = \frac{\int_0^{r_p}\rho^2 R_{NH_3}(y^s_{N_2}, T)\,d\rho}{R_{NH_3}(y_{N_2}, T)\int_0^{r_p}\rho^2\,d\rho}. \tag{3}$$

Catalyst particle:

$$\frac{1}{\rho^2}\frac{d}{d\rho}\left(\rho^2 N_{N_2}\right) = -\frac{1}{2}\frac{\alpha R_{NH_3}}{1-\epsilon}, \tag{4}$$

where

$$N_{N_2} = -\frac{CD_{eff}}{(1-2y^s_{N_2})}\frac{dy^s_{N_2}}{d\rho}. \tag{5}$$

Coolant (tube side)

$$\frac{dT_c}{dz} = \pm\frac{US}{\sum_i F_i c_{pi}}(T - T_c)$$

(+, cocurrent flow; −, countercurrent flow). (6)

Boundary conditions

Both flow schemes:

$$\text{at } r = r_1, \quad k_{er}\frac{\partial T}{\partial r} = U(T - T_c); \qquad \frac{\partial y_{N_2}}{\partial r} = 0$$

$$\text{at } r = r_2, \quad \frac{\partial T}{\partial r} = 0; \qquad \frac{\partial y_{N_2}}{\partial r} = 0$$

$$\text{at } \rho = 0, \quad \frac{dy^s_{N_2}}{d\rho} = 0$$

$$\text{at } \rho = r_p, \quad y^s_{N_2} = y_{N_2}. \tag{7}$$

Cocurrent flow (see Figure 1a):

$$\text{at } z = 0, \quad y_{N_2}(0) = y_{N_{2_0}}$$
$$T(0) = T_c(L_1)$$
$$T_c(0) = T_{c_0}. \tag{8a}$$

Countercurrent flow (see Figure 1b):

$$\text{at } z = 0, \quad y_{N_2}(0) = y_{N_{2_0}}$$
$$T(0) = T_c(0)$$
$$\text{at } z = L_1, \quad T_c(L_1) = T_{c_{L_1}}. \tag{8b}$$

Industrial autothermal reactors used for ammonia synthesis frequently include a heat exchanger to preheat the feed stream before it enters the cooling tubes. These arrangements are shown in Figures 2a and 2b for the cocurrent and countercurrent designs, respectively. The additional heat balances can be expressed as follows.

Heat exchanger

Tube side:

$$\frac{dT_t}{dz} = -\frac{S_{HE}U_{HE}}{\sum_i (F_i c_{pi})_t}(T_{sh} - T_t). \tag{9}$$

Shell side:

$$\frac{dT_{sh}}{dz} = -\frac{S_{HE}U_{HE}}{\sum_i (F_i c_{pi})_{sh}}(T_{sh} - T_t). \tag{10}$$

Boundary conditions

Cocurrent flow (see Figure 2a)

$$\text{at } z = 0, \quad y_{N_2}(0) = y_{N_{2_0}}$$
$$T(0) = T_c(L_1)$$
$$T_c(0) = T_t(L_1)$$
$$\text{at } z = L_1, \quad T(L_1) = T_{sh}(L_1)$$
$$\text{at } z = L_2, \quad T_t(L_2) = T_{t_{L_2}}. \tag{11a}$$

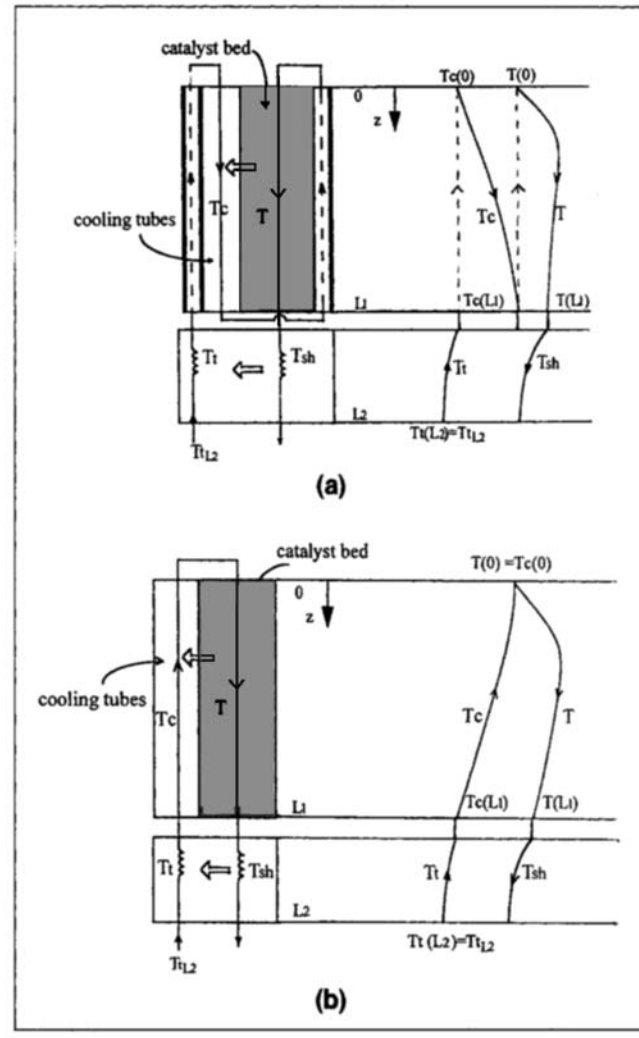

Figure 2. Reactor–heat exchanger: (a) cocurrent coolant flow; (b) countercurrent coolant flow.

Countercurrent flow (see Figure 2b):

$$\text{at } z = 0, \quad y_{N_2}(0) = y_{N_{2_0}}$$
$$T(0) = T_c(0)$$
$$\text{at } z = L_1, \quad T(L_1) = T_{sh}(L_1)$$
$$T_c(L_1) = T_t(L_1)$$
$$\text{at } z = L_2, \quad T_t(L_2) = T_{t_{L_2}}. \tag{11b}$$

The intrinsic rate of reaction used in the model was reported by Dyson and Simon (1968), which is a slightly modified form of the Temkin (1950) expression:

$$R_{NH_3} = k_2\left[K^2 f_{N_2}\left(\frac{f^3_{H_2}}{f^2_{NH_3}}\right)^{0.5} - \left(\frac{f^2_{NH_3}}{f^3_{H_2}}\right)^{0.5}\right], \tag{12}$$

where $k_2 = 4.914\ 10^{11}\ e^{-170{,}560.8/RT}$ and $f_i = \phi_i y_i P$ (Dyson and Simon, 1968).

Table 1. Physical Properties and Data Used in the Simulations

*Reactor**	
r_p (m)	0.00285
V_L (m^3)	4.07
L_1 (m)	5.18
N_t	84
d_o (m)	0.0508
d_i (m)	0.0381
$y_{N_{2_0}}$	0.219
$y_{H_{2_0}}$	0.65
$y_{NH_{3_0}}$	0.052
y_{inert}	0.079
P (atm)	286
V_e (s^{-1})	3.8333
$U^{-1} = h_w^{-1} + h_o^{-1}$	
h_w, k_{er} calculated using correlations reported by Dixon and Cresswell (1979).	
h_o estimated from the Colburn equation (Perry and Chilton, 1982).	
*Heat Exchanger***	
L_{HE} (m)	1
N_t	1158
d_o (m)	0.014
N_{bf}	9
U_{HE} calculated using the Colburn equation (Perry and Chilton, 1982) (tube side) and correlation reported by Donohue (1949) (shell side).	

*Data reported by Baddour et al., 1965 and Murase et al., 1970.
**Data reported by Elnashaie et al., 1988.

The equilibrium constant K was calculated from the expression given by Gillespie and Beattie (1930). The geometrical parameters and data used in the simulations are included in Table 1. To solve the mathematical model the radial coordinate for the catalyst bed was discretized, leading to a set of ODEs. The radial coordinate for the catalyst particle was also discretized by means of orthogonal collocation. The nonlinear algebraic equations corresponding to the catalyst particle were solved at each axial and radial position of the catalyst bed in order to calculate a local effectiveness factor. A quasi-Newton method was utilized in the solution. The equations corresponding to the gas phase (catalyst bed, coolant tubes, and heat exchanger) were finally integrated by means of a Gear algorithm. According to the boundary conditions, the equations for both autothermal designs (counter- and cocurrent schemes) constitute boundary-value problems, which were solved iteratively using the shooting method.

Results and Discussion

Existence of multiple steady states in the autothermal cocurrent reactor

In this section, the steady-state behavior of the autothermal cocurrent reactor is considered, neglecting the influence of the heat exchanger located at the bottom of the reactor (see Figure 1a). Thus, the mathematical model corresponds to Eqs. 1 to 7 with boundary conditions given by Eq. 8a.

In Figure 3, the exit coolant temperature is plotted against the inlet coolant temperature, for the operating conditions of Table 1 and three different space velocities. Curves corresponding to $V_e = 3.83$ s^{-1} (nominal value) and $V_e = 1.92$ s^{-1} show zones where three different values of $T_c(L_1)$ can be obtained for the same value of the inlet coolant temperature

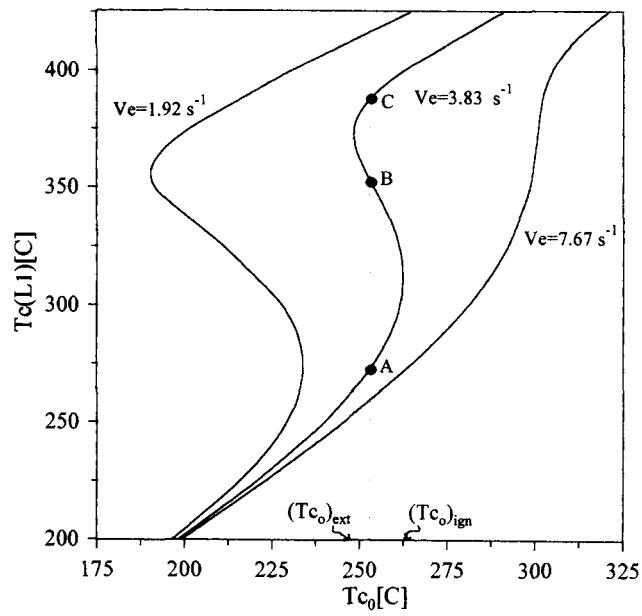

Figure 3. Autothermal cocurrent reactor.
Outlet coolant temperature vs. inlet coolant temperature, for different space velocities.

(T_{c_0}). It is important to note that $T_c(L_1)$ always coincides with $T(0)$ (see Figure 1a). Therefore, the autothermal cocurrent reactor could be operated under three different steady states for the same inlet conditions. An important hysteresis loop appears, which becomes less pronounced as the space velocity increases. Only in cases of very high space velocities (e.g., $V_e = 7.67$ s^{-1} in Figure 3) do the curves not present the characteristic S-shape. A case of steady-state multiplicity is illustrated in Figure 3 by means of points A, B, and C, corresponding to $V_e = 3.83$ s^{-1} and $T_{c_0} = 253$°C. The axial temperature profiles corresponding to these steady states are shown in Figure 4. For each steady state, four temperature profiles at different radial locations of the catalyst bed (shell side) have been plotted. The respective coolant temperature profiles (tube side) have also been included in the figure. In the lowest steady state (point A) the reaction level is low; therefore, the temperature increases slightly along the axial position, and the radial gradients are small. It should be noted that in the highest steady state (point C) all the axial temperature profiles show a maximum. The hot spots are higher and are located closer to the reactor inlet as the radial position increases (that is, as the distance from the tube wall increases). The radial temperature gradients are significant, particularly in those axial positions where high reaction rates and large temperature differences between reactants and coolant exist. Finally, the temperature profiles corresponding to steady-state B show an intermediate behavior. This steady state cannot be reached using a conventional startup procedure, because of the just-mentioned hysteresis loop (see Figure 3). As in case of the autothermal countercurrent reactor (van Heerden, 1953; Baddour et al., 1965), the intermediate steady states found in the autothermal cocurrent design should also be unstable. An analysis of stability should be carried out to confirm this presumption.

The maximum temperature reached in the catalyst bed and the molar fraction of ammonia at the reactor outlet have been

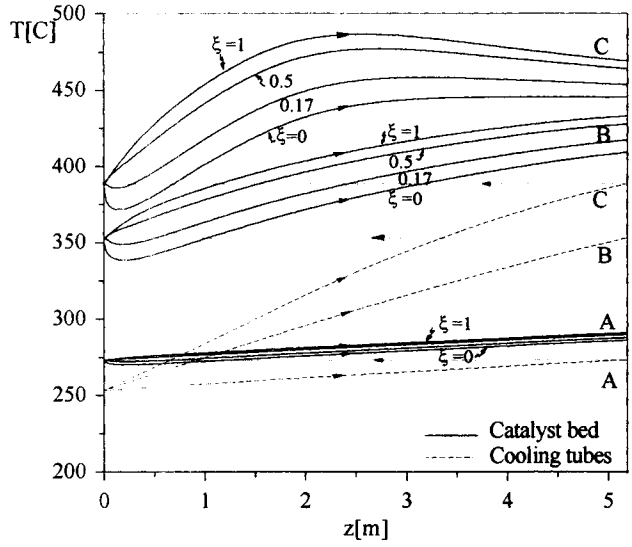

Figure 4. Axial temperatures at different radial locations (catalyst bed) with corresponding coolant temperatures for steady states *A*, *B*, and *C* of Figure 3.

plotted as a function of T_{c_0} in Figure 5. Points *A*, *B*, and *C* corresponding to Figure 3 are also indicated. Both curves show the typical S-shape, but the molar fraction of NH_3 reaches a maximum at a given point corresponding to the upper branch. Beyond this *optimal operating point* the conversion increases as T_{c_0} increases, because the reverse reaction is gradually favored with the temperature rise. The optimal operating point is close to the blowout temperature, which again is similar to the results reported by Baddour et al. (1965) for the autothermal countercurrent reactor. Under these conditions, a small decrease in the value of the inlet coolant temperature may cause the reactor to move to a lower (extinguished) steady state. However, as the curve is almost

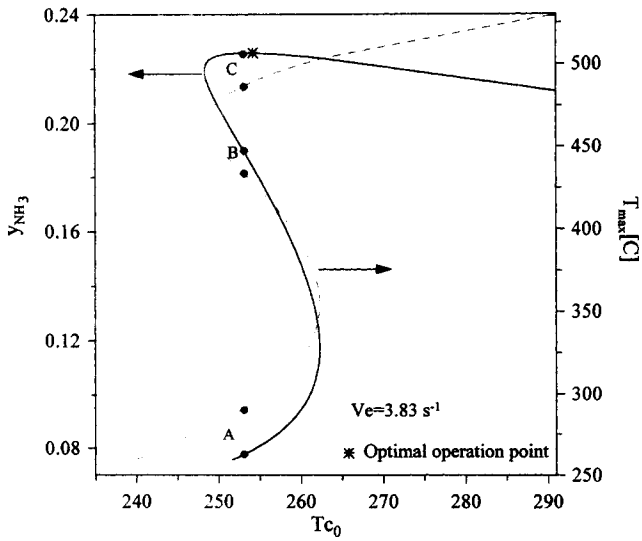

Figure 5. Maximum temperature of the catalyst bed (at $\xi = 1$) and outlet molar fraction of ammonia, as affected by the inlet coolant temperature.

flat near the optimum point, a shift of the operating point to the right would not introduce a significant reduction in the yield of NH_3.

At this point, it is appropriate to discuss the differences between the results of the present article and those reported by Degnan and Wei (1979). As mentioned, these researchers analyzed the steady-state behavior of the autothermal cocurrent reactor by means of a homogeneous one-dimensional model. By assuming an irreverible single reaction with the power-law kinetic model, the authors did not find steady-state multiplicity in the cocurrent reactor for a wide range of operating conditions. In fact, unlike the curves shown in Figure 3 of this article, the analogous curves presented by Degnan and Wei (1979) are not S-shaped, even for long residence times (i.e., low space velocities). The apparent contradiction between both results can be explained as follows. Degnan and Wei analyzed the parametric sensitivity and stability of the autothermal cocurrent reactor subject to *specified* temperatures for reactants and coolant at the axial position $z = 0$. In other words, $T(0)$ and $T_c(0)$ were independently fixed, because the authors were mainly focused on the attainment of isothermal temperature profiles in the catalyst bed. Under the inlet conditions fixed by Degnan and Wei, the boundary-value problem defined by Eqs. 8a becomes an initial-value problem, similar to that found in the *not-autothermal* cocurrent reactor (Borio et al., 1995). However, these are not strictly the inlet conditions of the *autothermal* cocurrent reactor, because the gas temperature at the inlet of the catalyst bed is a consequence of the gas temperature at the outlet of the cooling tubes. Therefore, the value of $T(0)$ cannot be specified independently [i.e., $T(0) = T_c(L_1)$; see Figure 1a]. The mass transport toward the inlet of the catalyst bed, which is *inherent* to autothermal reactors, is accompanied by heat transport. This feedback of heat produces in the autothermal cocurrent reactor an ignition-extinction phenomenon similar to that found in the countercurrently cooled reactor. It is important to note that the reactor model and the kinetic expression used in the present article are different from those reported by Degnan and Wei (1979). However, we have also found multiple steady states in the cocurrent autothermal reactor for the case of homogeneous one-dimensional model and irreversible first-order reaction, provided that the appropriate boundary conditions (Eqs. 8a) are adopted. Conversely, the *not-autothermal* cocurrent reactor is unconditionally stable (Borio et al., 1989), because the feedback of heat does not occur.

Influence of the operating variables on the stability of the autothermal cocurrent reactor: Comparison with the autothermal countercurrent reactor

Different parameters or operating conditions can affect the stability of the autothermal cocurrent reactor. Just a few will be analyzed here. The influence of the space velocity is shown in Figure 3. The ignition temperature $(T_{c_0})_{ign}$ and the extinction (or blowout) temperature $(T_{c_0})_{ext}$ are indicated for $V_e = 3.83\ s^{-1}$. It is important to note that both temperatures increase with the space velocity, which is analogous to the results reported by Baddour et al. (1965) for the countercurrent reactor. This effect can be observed in Figure 6, where the inlet coolant temperatures corresponding to the ignition and

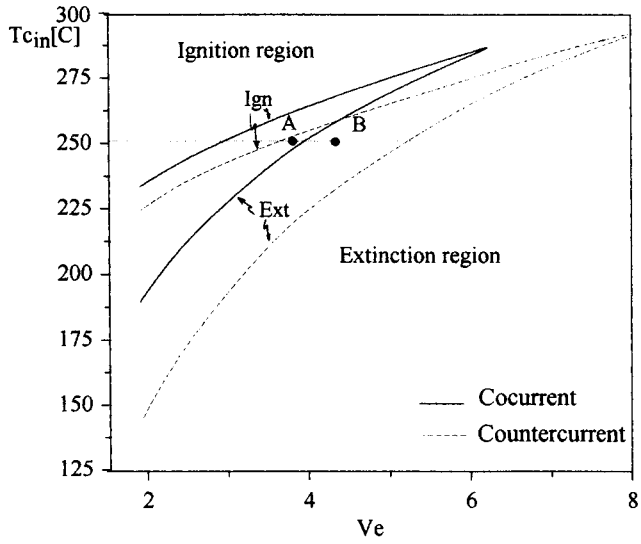

Figure 6. Ignition and extinction temperatures as affected by the space velocity.

$T_{c_{in}} = T_{c_0}$ for cocurrent flow; $T_{c_{in}} = T_{c_{L_1}}$ for countercurrent flow.

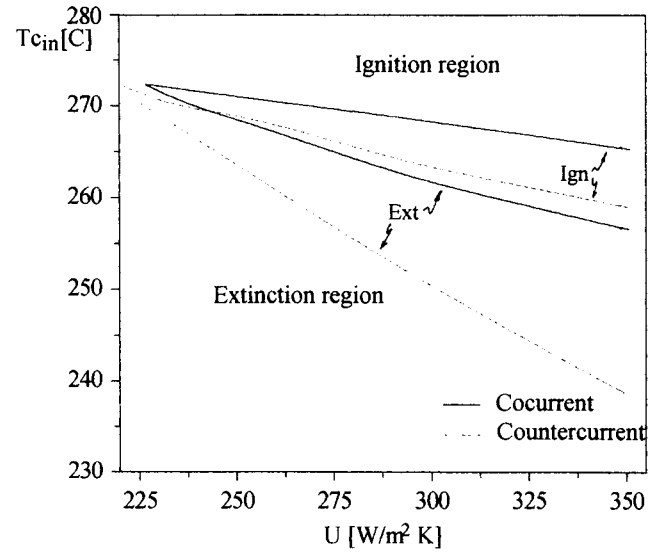

Figure 7. Ignition and extinction temperatures as affected by the overall heat-transfer coefficient in the reactor.

$T_{c_{in}} = T_{c_0}$ for the cocurrent reactor; $T_{c_{in}} = T_{c_{L_1}}$ for the countercurrent reactor.

extinction points are plotted as a function of the space velocity, for the cooling schemes shown in Figures 1a and 1b. The shape usually seen in a cusp bifurcation is evident. Beyond the cusp point, which is located at $V_e = 6.28\ s^{-1}$, the reactor shows uniqueness. The broad region between both branches corresponds to operating conditions for which the cocurrent reactor presents three steady states. When an increase in the space velocity occurs, the respective increase in the blowout temperature can lead the reactor to extinction, provided that the remaining operating conditions are kept constant (e.g., points A and B in Figure 6). This is particularly important when an ammonia synthesis converter is being operated, because the optimal point is not far from the blowout point (see Figure 5). Finally, the countercurrent reactor has a cusp point for a space velocity higher than that of the cocurrent case (see Figure 6). Thus, for each value of V_e the differences between the ignition and extinction temperatures for the countercurrent reactor are higher than those found in the cocurrent case.

The influence of the overall heat-transfer coefficient in the reactor on the steady-state regions is shown in Figure 7, for both the cocurrent and countercurrent configurations. The cusp point is located at $U = 226\ W/(m^2 \cdot K)$ for the cocurrent case. As already seen, the ignition and extinction temperatures are higher in the cocurrent reactor and the region where steady-state multiplicity exists is smaller. When a decrease in the value of U occurs (e.g., by continuous fouling of the cooling tubes), the inlet coolant temperature ($T_{c_{in}}$) may become lower than the blowout temperature, with the consequent extinction of the reactor.

Finally, the influence of the catalyst activity on the steady-state regions for both reactor designs is shown in Figure 8. As an approximation, a constant activity coefficient (α) was assumed along the axial and radial coordinates. The cocurrent design shows multiplicity for activity coefficients higher than 0.55. Ignition and extinction temperatures increase as the catalyst activity coefficient decreases. Again, the reactor becomes extinct when an important loss in the catalyst activity occurs, due to the increase in the blowout temperature.

Influence of the heat exchanger on the reactor stability

Industrial autothermal reactors frequently include a heat exchanger to complete the preheating of the feed mixture up to the reaction temperature. The heat exchange between the streams of products and feed introduces an additional feedback of heat that in turns affects the reactor stability. The results to be shown in this section were obtained by solving the mathematical model composed by Eqs. 1–6 and 9–10,

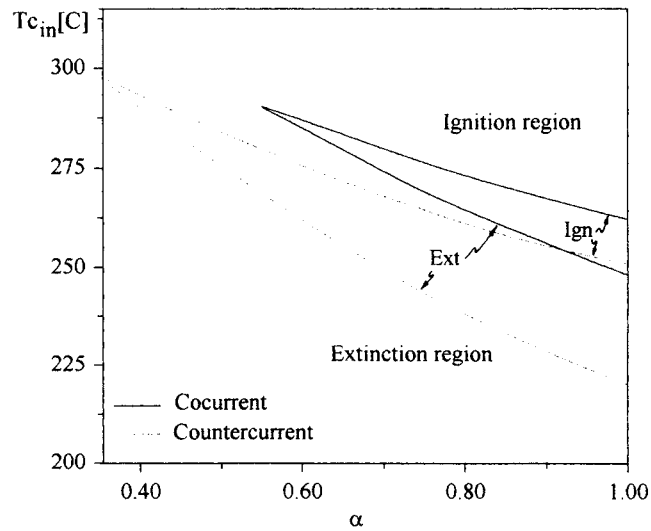

Figure 8. Ignition and extinction temperatures as affected by the catalyst activity.

$T_{c_{in}} = T_{c_0}$ for the cocurrent reactor; $T_{c_{in}} = T_{c_{L_1}}$ for the countercurrent reactor.

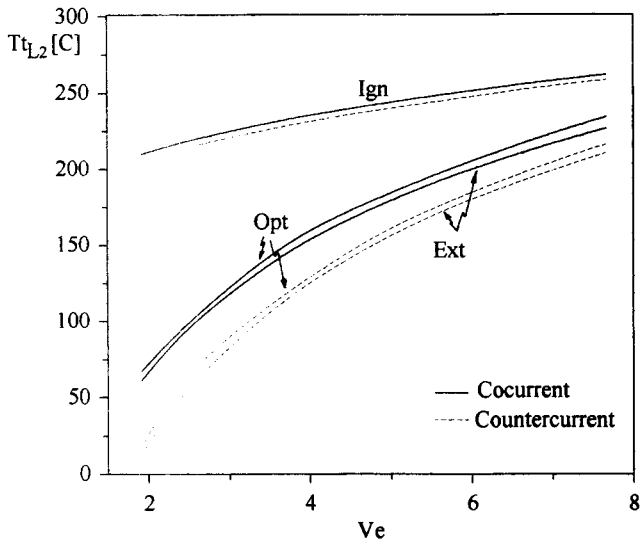

Figure 9. Reactor–heat exchanger.

Ignition, extinction, and optimal temperatures as affected by the space velocity, for the autothermal cocurrent and countercurrent designs.

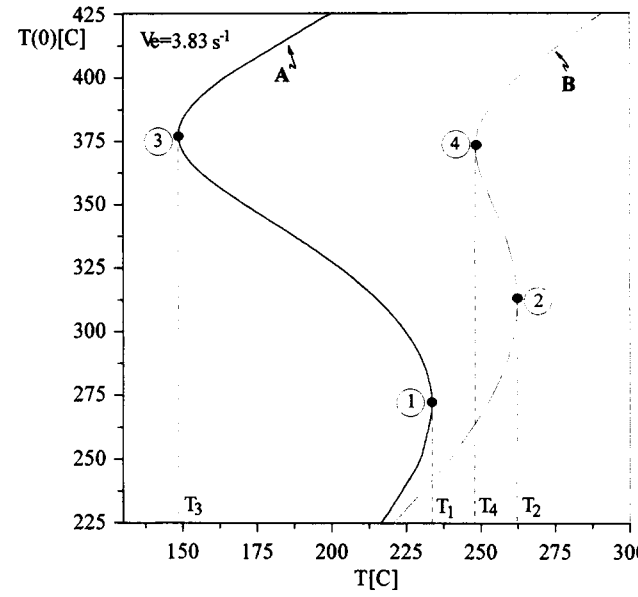

Figure 10. Autothermal cocurrent design.

Temperature at the top of the reactor as affected by $T_{t_{L_2}}$ (curve A) or by T_{c_0} (curve B).

subject to the boundary conditions given either by Eqs. 7 and 11a (cocurrent) or 7 and 11b (countercurrent).

Considering the reactor and the heat exchanger as a unique system, the new manipulated variable (instead of T_{c_0}) is the inlet temperature to the heat exchanger ($T_{t_{L_2}}$). Thus, the values of ($T_{t_{L_2}}$) at the ignition and the extinction points are displayed in Figure 9 for the cocurrent and countercurrent schemes. As shown, the regions of multiple steady states are now remarkably larger than those found in Figure 6, because the cusp points shifted to the right. The ignition and extinction temperatures differ considerably due to the influence of the heat exchanger. As in Figure 6, the extinction temperatures corresponding to the cocurrent reactor are higher than those of the countercurrent reactor. The optimal inlet temperatures (corresponding to maximum concentration of ammonia at the reactor outlet) are also included in Figure 9. For both coolant-flow schemes, the optimal operating points are located near the blowout conditions.

The addition of a heat exchanger introduces a significant displacement of the reactor ignition point. This phenomenon can be appreciated in Figure 10, where the temperature at the top of the reactor, $T(0)$, is plotted against the manipulated variable, $T_{t_{L_2}}$ (curve *A*). For comparative purposes, $T(0)$ is also plotted vs. T_{c_0}, which becomes the manipulated variable when the heat exchanger is not taken into account (curve *B*). The ignition conditions are indicated as point 1 (considering the influence of the heat exchanger) and point 2 (without considering the heat exchanger). The value of the temperature T_1 (234°C) is significantly lower than the value of T_2 (around 267°C). Still more pronounced are the differences between the extinction temperatures T_3 and T_4. These results are extended to a wider range of operating conditions in Figure 11, where the values of the ignition and extinction temperatures are plotted against the space velocity for the autothermal cocurrent design. Both the system reactor–heat exchanger and the reactor alone have been considered. Points 1 to 4 of Figure 10 are also indicated in Figure 11. The system *reactor–heat exchanger* shows substantially lower ignition temperatures than those corresponding to the reactor alone. The reason for the reduction of the ignition temperature is the additional amount of heat being transferred in the heat exchanger, which contributes to an easier *ignition* of the catalyst bed. Also the differences between ignition and extinction temperatures are clearly bigger for the combined reactor–heat exchanger system, which tends to stabilize the reactor operation.

Conclusions

- Unlike the *not-autothermal* cocurrent reactor, which is unconditionally stable, the *autothermal* cocurrent reactor shows steady-state multiplicity for a broad range of operating

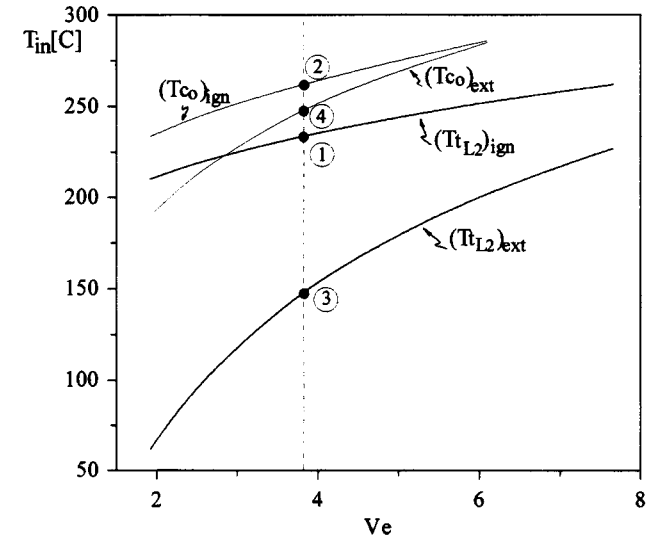

Figure 11. Autothermal cocurrent design.

Influence of the heat exchanger on the ignition and extinction temperatures: $T_{in} = T_{t_{L_2}}$ for the reactor–heat exchanger system; $T_{in} = T_{c_0}$ for the reactor alone.

conditions. This phenomenon had not been reported in the literature.

- The steady-state multiplicity does not arise from the mutual direction between the streams of reactants and coolant. It is the result of the mass transport from the back to the front of the catalyst bed. This feedback of mass, which is associated with a feedback of heat, is the source of the reactor instability.
- The reactor stability diminishes (that is, the blowout temperature increases) as the space velocity increases and the overall heat-transfer coefficient (or the catalyst activity) decreases.
- For all the parameters investigated, the regions where multiple steady states occur are smaller for the cocurrent reactor than for the countercurrent reactor.
- The existence of a heat exchanger at the bottom of the reactor introduces important displacements of the cusp points and increases the differences between the ignition and extinction temperatures.

Additional studies should be carried out, aiming at confirming experimentally the existence of multiple steady states in autothermal cocurrent reactors, and at exploring the reactor operation under unsteady-state conditions.

Notation

c_{pi} = specific heat of component i, kJ/(kmol·K)
C = total molar concentration, kmol/m^3
D_{eff} = effective diffusivity of nitrogen (catalyst particle), m^2/s
D_{er} = effective radial diffusivity of nitrogen, m^2/s
d_i, d_o = internal and external diameters of the tubes, m
f_i = fugacity of component i in the mixture, kPa
F_i = molar flow of component i, kmol/s
G = specific mass flow rate, kg/(m^2·s)
h_w = wall heat-transfer coefficient, kW/(m^2·s)
h_o = heat-transfer coefficient (tube side), kW/(m^2·K)
k_2 = reaction-rate constant for decomposition of ammonia, kmol$_{NH_3}$ kPa$^{1/2}$/(m^3·s)
k_{er} = effective radial heat conductivity, kW/(m·K)
L_{HE} = length of the heat exchanger, m
L_1 = reactor length, m
$L_2 = L_1 + L_{HE}$, m
M = average molecular weight, kg/kmol
N_{N_2} = specific molar flow, kmol$_{N_2}$/(m^2·s)
N_{bf} = number of baffles in the heat exchanger
N_t = tube number
P = reactor pressure, kPa
r = radial coordinate (catalyst bed), m
r_p = equivalent radius of the catalyst particle, m
r_1 = external radius of the cooling tubes (inner radius of equivalent annular area), m
r_2 = external radius of the equivalent annular area, m
R = universal gas constant, kJ/(kmol·K)
R_{NH_3} = intrinsic reaction rate, kmol$_{NH_3}$/(m^3·s)
S = heat-transfer area per unit length, m^2/m
T_c = coolant temperature, K
T_{sh} = temperature at the heat exchanger (shell side), K
U = overall heat-transfer coefficient, kW/(m^2·K)
V_L = total catalyst volume, m^3
y_i = molar fraction of component i (gas phase)
y_i^s = molar fraction of component i (catalyst particle)

Greek letters

ϵ = porosity, m^3/m^3
ΔH_r = heat of reaction, kJ/kmol$_{NH_3}$
η = effectiveness factor
ϕ_i = fugacity coefficient of component i
$\xi = (r - r_1)/(r_2 - r_1)$, dimensionless radial coordinate (catalyst bed)
ρ = radial coordinate (catalyst particle), m

Subscripts

HE = heat exchanger
in = inlet
L_1 = at axial position, $z = L_1$
L_2 = at axial position, $z = L_2$
max = maximum
opt = optimal
sh = shell side (heat exchanger)
t = tube side (heat exchanger)
0 = at axial position, $z = 0$

Literature Cited

Ampaya, J. P., and R. G. Rinker, "Autothermal Reactor with Internal Heat Exchange—I. Numerical and Experimental Studies in the Multiple Steady-State Region," *Chem. Eng. Sci.*, **32**, 1327 (1977).

Baddour, R. F., P. L. T. Brian, B. A. Logeais, and J. P. Eymery, "Steady-State Simulation of an Ammonia Synthesis Converter," *Chem. Eng. Sci.*, **20**, 281 (1965).

Borio, D. O., J. E. Gatica, and J. A. Porras, "Wall-Cooled Fixed-Bed Reactors: Parametric Sensitivity as a Design Criterion," *AIChE J.*, **35**(2), 287 (1989).

Borio, D. O., V. Bucalá, and J. A. Porras, "Thermal Regimes in Cocurrently Cooled Fixed-Bed Reactors," *Chem. Eng. Sci.*, **50**(19), 3115 (1995).

Chylla, R. W., Jr., R. A. Adomaitis, and A. Cinar, "Stability of Tubular and Autothermal Packed Bed Reactors Using Phase Plane Analysis," *Ind. Eng. Chem. Res.*, **26**, 1356 (1987).

Degnan, T. F., and J. Wei, "The Cocurrent Reactor Heat Exchanger: Part I. Theory," *AIChE J.*, **25**(2), 338 (1979).

Degnan, T. F., and J. Wei, "The Cocurrent Reactor Heat Exchanger: Part II. Experimental Results," *AIChE J.*, **26**(1), 60 (1980).

Dixon, A. G., and D. L. Cresswell, "Theoretical Prediction of Effective Heat Transfer Parameters in Packed Beds," *AIChE J.*, **25**(4), 663 (1979).

Donohue, D. A., "Heat Transfer and Pressure Drop in Heat Exchangers," *Ind. Eng. Chem.*, **41**, 2499 (1949).

Dyson, D. C., and J. M. Simon, "A Kinetic Expression with Diffusion Correction for Ammonia Synthesis on Industrial Catalyst," *Ind. Eng. Chem. Fund.*, **7**(4), 605 (1968).

Eigenberger, G., "Stability and Dynamics of Heterogeneous Catalytic Systems," *Int. Chem. Eng.*, **21**(1), 17 (1981).

Elnashaie, S. E. E. H., A. T. Mahfouz, and S. S. Elshishini, "Digital Simulation of an Industrial Ammonia Reactor," *Chem. Eng. Process.*, **23**, 165 (1988).

Fodor, L., "Actual Optimization Problems of the Reactors used for Ammonia Synthesis," *Chem. Ind.-Génie Chim.*, **104**(8), 1002 (1971).

Gillespie, L. J., and J. A. Beattie, *Phys. Rev.*, **36**, 743 (1930).

Inoue, H., and Komiya H., "On the Stability of Autothermal Reactors," *Int. Chem. Eng.*, **8**(4), 749 (1968).

Li, H., R. R. Hudgins, and K. S. Chang, "Equivalent Annular Model of a Multitubular Shell-Side (MSS) Fixed-Bed Reactor," *AIChE J.*, **37**(8), 1129 (1991).

Lovo, M., and V. Balakotaiah, "Multiplicity Features of Nonadiabatic Autothermal Tubular Reactors," *AIChE J.*, **38**(1), 116 (1992).

Lovo, M., and V. Balakotaiah, "On the Steady-State Behavior of the Nonadiabatic Autothermal Tubular Reactor," *Chem. Eng. Sci.*, **49**(23), 3861 (1994).

Luss, D., and P. Medellin, "Steady-State Multiplicity and Stability in a Countercurrently Cooled Tubular Reactor," *Proc. Eur. Symp. on Chem. React. Eng.*, Amsterdam, p. B4-47 (1972).

Murase, A., H. L. Roberts, and A. O. Converse, "Optimal Thermal Design of an Autothermal Ammonia Synthesis Reactor," *Ind. Eng. Chem. Process Des. Dev.*, **9**(4), 503 (1970).

Pedernera, M., D. O. Borio, and J. A. Porras, "A New Cocurrent Reactor for Ammonia Synthesis," *Chem. Eng. Sci.*, **51**(11), 2927 (1996).

Perry, R. H., and C. H. Chilton, *Manual del Ingeniero Químico*, 5th ed., Vol. 1, McGraw-Hill, New York (1982).

Temkin, M., *J. Phys. Chem. (USSR)*, **24**, 1312 (1950).

van Heerden, C., "Autothermal Processes. Properties and Reactor Design," *Ind. Eng. Chem.*, **45**(6), 1242 (1953).

Manuscript received Jan. 16, 1996, revision received June 10, 1996.